Applied Ocean Research 43 (2013) 206–213

Contents lists available at ScienceDirect

Applied Ocean Research

journal homepage: www.elsevier.com/locate/apor

# Flap gate farm: From Venice lagoon defense to resonating wave energy production. Part 1: Natural modes

P. Sammarco*, S. Michele, M. d'Errico

*Department of Civil Engineering and Computer Science, Università degli studi di Roma Tor Vergata, Via del Politecnico 1, 00133 Roma, Italy*

ARTICLE INFO

*Article history:*
Received 6 July 2013
Received in revised form 19 September 2013
Accepted 1 October 2013

*Keywords:*
Flap gate energy
Wave–body interaction
Eigenmodes

ABSTRACT

We consider a flap-gate farm, i.e. a series of $P$ arrays, each made by $Q$ neighboring flap gates, in an infinitely long channel. We show that there are $P \times (Q-1)$ natural modes and determine their eigenfrequencies and modal forms. When the distance between the arrays goes to infinity the eigenfrequencies converge to the $Q-1$ values given by Li and Mei [14]. For an ad-hoc combination of channel geometry and flap gate characteristics, modal excitation can give significantly larger response than for the case of a single or a sparse gate system. This aspect is relevant for the design of an optimal gate farm wave energy converter.



## 1. Introduction

The attention to ocean waves as an energy resource has been high since after the II World War. Many types of wave energy converter (WEC) have been ingeniously designed and sometimes prototyped [1,2]. They are all based on the mechanical principle of maximizing the fractional quota of power that can be extracted from the incoming waves. One family of these devices includes flap gates hinged on a bottom axis and they oscillate in unison with the waves [3]. The mechanical principle of these devices is the mass-spring-damped forced oscillator, exactly the same of the floating gates already designed in the eighties by the Consorzio Venezia Nuova [4] to protect Venice Lagoon from flooding. In the case of a flap-gate WEC the difference from the Venice gates is in the purpose, which is to maximize the oscillation amplitude of the gates to be transformed into electricity by mechanical coupling.

The research developed so far has focused on the behavior of an isolated gate in a channel [56] or in the open ocean [7], and a sparse gate system [8,9]. However, when the gates are non-sparse, it is exactly the theory and experimental evidence developed for the Venice gates case that suggest a new type of WEC based on resonating wave–structure interaction. Indeed, for one array of neighboring gates aligned on a common axis, flume experiments have revealed that at certain frequencies $\omega$ of the incoming waves the gates can be excited to oscillate in opposite phase at frequencies $\omega/2$ [4] with a very large oscillation amplitude. Mei et al. [10] have identified this resonance mechanism showing the existence of trapped modes. As in the case of edge waves on a beach, if the gates are in a channel, resonance is possible through a nonlinear subharmonic mechanism as shown by Sammarco et al. [11,12]. If the gate barrier is not confined in a channel, but open to sea, radiation is possible and trapping is imperfect: a linear synchronous resonance mechanism is then possible. The linear theory of Adamo and Mei [13] clearly resolves the case of a semi-infinite channel on one side of the barrier and a semi-infinite domain on the other.

For one array made by $Q$ identical gates spanning the full width of an infinitely long channel, Li and Mei [14] have determined all the $Q-1$ natural modes. Panizzo et al. [15] analyzed several experimental data set for spectral waves by means of the empirical orthogonal function (EOF) method. They showed that modal excitation of the gate array is always present in real seas, when the natural frequencies fall within the wave spectrum frequency range. Therefore an extremely efficient WEC can be designed to have a large number of eigenfrequencies all falling within the given wave spectrum of interest. To this end we define a "gate farm": a series of $P$ arrays each made of $Q$ articulated neighboring gates hinged on a common axis. The Venice barrier case of Li and Mei [14] is the special case $P=1$. We show that there are $P \times (Q-1)$ natural frequencies and associated modal forms. We also show that when the distance $L$ between arrays increases, the eigenfrequencies converge to the $Q-1$ values of Li and Mei [14]. We also investigate the case of in-phase motion of each single array, i.e. when the gates of each array are locked. In Section 2 the geometrical parameters of the system are defined and the governing equations and associated boundary conditions are given. In Sections 3 and 4, solutions are found respectively for the out-of-phase motion and for the in-phase motion. In Section 5 a numerical analysis shows how the gate farm can be designed to maximize wave trapping and therefore maximize gates motion and wave energy extraction.

* Corresponding author. Tel.: +39 0672597020
*E-mail address:* sammarco@ing.uniroma2.it (P. Sammarco).

0141-1187/$ - see front matter © 2013 Elsevier Ltd. All rights reserved.
http://dx.doi.org/10.1016/j.apor.2013.10.001

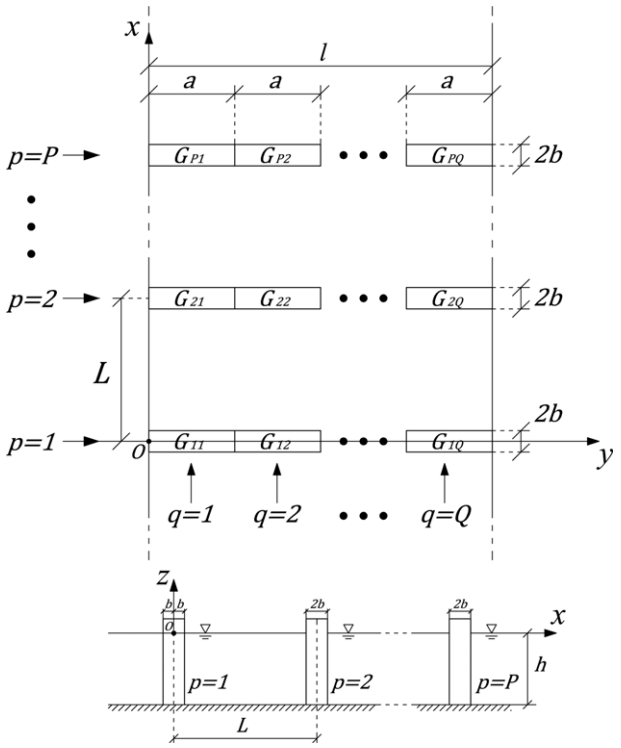


**Fig. 1.** Plan geometry and side view.

## 2. Governing equations for the $P \times Q$ gate farm

As shown in Fig. 1, there are $P$ arrays of neighboring gates. Each array, $p = 1,..., P$, is composed of a series of $Q$ floating gates ($q = 1, 2,...Q$) and spans the full width $l$ of an infinitely long channel. All the gates are identical. Let $a$ and $2b$ indicate respectively width and thickness of the single gate; then $l = Qa$. The symbol $G_{pq}$ denotes the $q$th gate of the $p$th array, while $\Theta_{pq}$ indicate the angular displacement of $G_{pq}$, positive if clockwise. We choose a three dimensional Cartesian coordinate system where the $x$ and $y$ axes lie on the mean free surface and the $z$-axis points vertically upward. The $y$-axis bisects the first array ($p = 1$), while the $x$-axis coincides with the left bank of the channel. The gates of each array $p = 1,..., P$, are hinged along a common axis lying on $x = (p-1)L, z = -h$.

Let $\Theta_p(y, t)$ indicate the angular displacement function of the $p$th array:

$$\Theta_p(y,t) = \{\Theta_{pq}(t)\} = \{\Theta_{p1}(t), \ldots, \Theta_{pQ}(t)\}. \tag{1}$$

$\Theta_p(y, t)$ is a piece-wise constant function of $y$. The analysis is performed in the framework of irrotational flow and small-amplitude oscillations. The velocity potential $\Phi$ must satisfy the Laplace equation in the fluid domain:

$$\nabla^2\Phi = 0, \tag{2}$$

have zero normal velocity both on the seabed:

$$\frac{\partial\Phi}{\partial z} = 0, \quad z = -h, \tag{3}$$

and on the vertical banks of the channel:

$$\frac{\partial\Phi}{\partial y} = 0, \quad y = 0, \ y = l. \tag{4}$$

On the sea surface, the flow must be tangential and the pressure equals to the atmospheric; hence, the boundary condition is:

$$\frac{\partial^2\Phi}{\partial t^2} + g\frac{\partial\Phi}{\partial z} = 0, \quad z = 0. \tag{5}$$

Let $\Phi^{\mp}$ indicate the solution in the two semi-infinite parts of the channel, respectively in $x \in (-\infty, -b]$ and $x \in [(P-1)L + b, +\infty)$, $y \in [0, l]$, $z \in [-h, 0]$. Also, let $\Phi^p$ indicate the potential in the part of fluid domain between the array $p$ and the array $p + 1$. With this notation we can specify the kinematic boundary condition on the $P$ arrays. On the $p = 1$ array the kinematic boundary condition is:

$$\begin{aligned} \frac{\partial\Phi^-}{\partial x} &= \frac{\partial\Theta_1}{\partial t}(z+h), \qquad x = -b, \\ \frac{\partial\Phi^1}{\partial x} &= \frac{\partial\Theta_1}{\partial t}(z+h), \qquad x = b, \end{aligned} \tag{6}$$

while on the $p = 2,..., P-1$, arrays we have:

$$\begin{aligned} \frac{\partial\Phi^{p-1}}{\partial x} &= \frac{\partial\Theta_p}{\partial t}(z+h), \qquad x = (p-1)L - b, \\ \frac{\partial\Phi^{p}}{\partial x} &= \frac{\partial\Theta_p}{\partial t}(z+h), \qquad x = (p-1)L + b, \end{aligned} \tag{7}$$

and finally on the $p = P$ array:

$$\begin{aligned} \frac{\partial\Phi^{P-1}}{\partial x} &= \frac{\partial\Theta_P}{\partial t}(z+h), \qquad x = (P-1)L - b, \\ \frac{\partial\Phi^{+}}{\partial x} &= \frac{\partial\Theta_P}{\partial t}(z+h), \qquad x = (P-1)L + b. \end{aligned} \tag{8}$$

Consider harmonic motion of frequency $\omega$:

$$\begin{aligned} \Phi(x,y,z,t) &= \mathrm{Re}\{\phi(x,y,z)e^{-i\omega t}\}, \\ \Theta_p(y,t) &= \mathrm{Re}\{\theta_p(y)e^{-i\omega t}\}. \end{aligned} \tag{9}$$

The potentials in each subdomain can be found by the method of separation of variables.

## 3. Out-of-phase motion: trapped modes

Solution for wave potential is found in each of the $P + 1$ subdomains; then the gate dynamics equations are solved.

### 3.1. $\phi^-, x \in (-\infty, -b], y \in [0, l], z \in [-h, 0]$

The governing equation and boundary conditions are:

$$\nabla^2\phi^- = 0, \qquad x \in (-\infty, -b], \tag{10a}$$

$$\frac{\partial\phi^-}{\partial y} = 0, \qquad y = 0, \ y = l, \tag{10b}$$

$$\frac{\partial\phi^-}{\partial z} = 0, \qquad z = -h, \tag{10c}$$

$$\frac{\partial\phi^-}{\partial z} - \frac{\omega^2}{g}\phi^- = 0, \qquad z = 0, \tag{10d}$$

$$\frac{\partial\phi^-}{\partial x} = -i\omega(z+h)\theta_1(y), \qquad x = -b, \tag{10e}$$

$$\phi^- \text{ bounded as } x \to -\infty. \tag{10f}$$

Let sh, ch and th indicate shorthand notation respectively for sinh, cosh and tanh. Solution of Laplace equation (10a) with boundary conditions (10b), (10c), (10d), (10e), and (10f) is given by:

$$\phi^- = \sum_{m=0}^{\infty}\sum_{n=0}^{\infty} B_{mn}e^{-i\alpha_{mn}x}\cos\frac{m\pi y}{l}\mathrm{ch}\,k_n(h+z), \tag{11}$$

where $k_n$ denotes the roots of the dispersion relation:

$$\begin{aligned} &\omega^2 = gk_0\,\mathrm{th}\,k_0h, \\ &\omega^2 = -g\bar{k}_n\tan\bar{k}_nh, \\ &k_n = i\bar{k}_n, \quad n = 1, \ldots, \infty, \end{aligned} \tag{12}$$

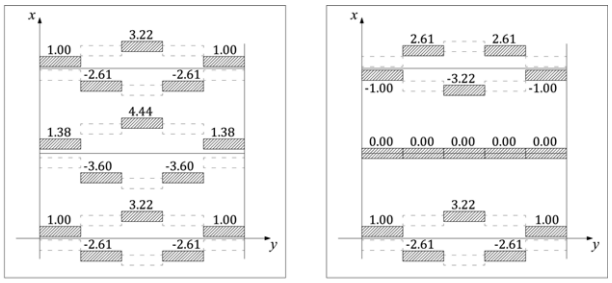


(a) $N_{11}$




(b) $N_{12}$

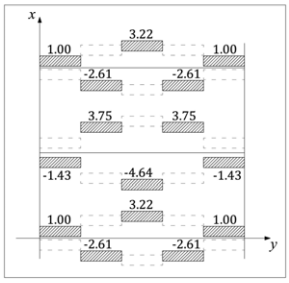


(c) $N_{13}$

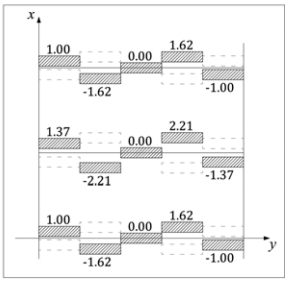


(d) $N_{21}$

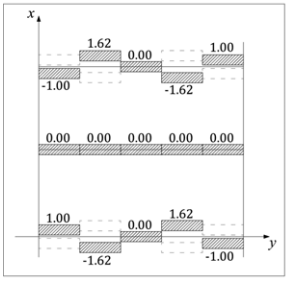


(e) $N_{22}$

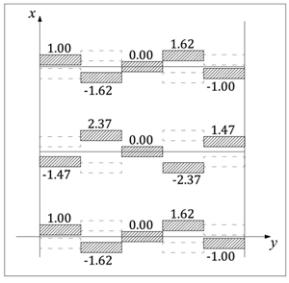


(f) $N_{23}$

**Fig. 2.** Modal profiles.

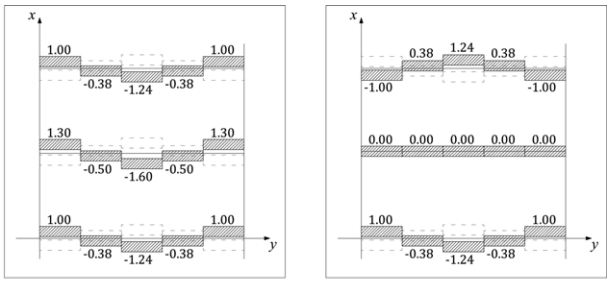


(a) $N_{31}$




(b) $N_{32}$

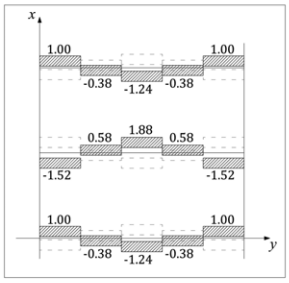


(c) $N_{33}$

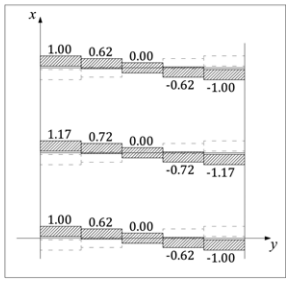


(d) $N_{41}$

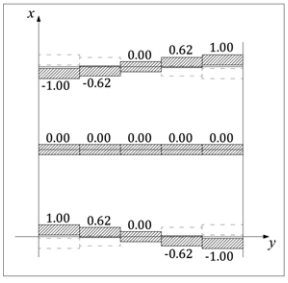


(e) $N_{42}$

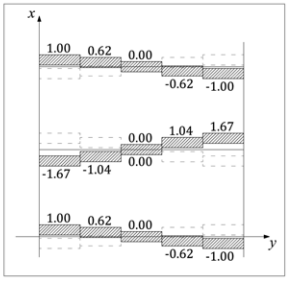


(f) $N_{43}$

**Fig. 3.** Modal profiles.

and $i$ denotes the imaginary unit. The coefficients $\alpha_{mn}$ are given by:

$$\alpha_{mn} = \sqrt{k_n^2 - \left(\frac{m\pi}{l}\right)^2}, \quad n, m = 0, ..., \infty. \tag{13}$$

According to $\omega$, $m$ and $n$, different types of waves are present:

| | | |
|---|---|---|
| $n = 0, m = 0,$ | $\alpha_{00} = k_0,$ | long crested propagating waves, |
| $n > 0, m = 0,$ | $\alpha_{0n} = i\bar{k}_n,$ | long crested evanescent waves, |
| $n = 0, m \le M,$ | $\alpha_{m0} = \sqrt{k_0^2 - \left(\frac{m\pi}{l}\right)^2},$ | short crested propagating waves, |
| $n = 0, m > M,$ | $\alpha_{m0} = i\bar{\alpha}_{m0} = i\sqrt{\left(\frac{m\pi}{l}\right)^2 - k_0^2},$ | short crested evanescent waves, |
| $n > 0, m > 0,$ | $\alpha_{mn} = i\bar{\alpha}_{mn} = i\sqrt{k_n^2 + \left(\frac{m\pi}{l}\right)^2},$ | short crested evanescent waves. |

$M$ is the largest integer that renders $\alpha_{m0}$ real, i.e. such that $k_0 > M\pi/l$. Application of the boundary condition (10e) on the left side ($x = -b$) of the array $p = 1$ yields the coefficient $B_{mn}$ of expression (11).

Recalling that:

$$\theta_1(y) = \{\theta_{1q}\} = \{\theta_{11}, \ldots \theta_{1Q}\}, \tag{14}$$

the condition:

$$\int_0^l \theta_1(y)\, dy = 0, \tag{15}$$

assures that there are no long-crested propagating and long-crested evanescent waves, i.e. $B_{0n} = 0$, $n = 0, 1, ..., \infty$.

$\phi^-$ must include only terms that decay exponentially as $x \to -\infty$ so that waves are trapped. As in Li and Mei [14], damping is not considered in eigenfrequency analysis and the sum that contains short-crested propagating waves ($n = 0, m = 1, ..., M$) to $-\infty$, if present, is excluded. Hence expression (11) becomes:

$$\begin{aligned}\phi^- = -i\omega \sum_{q=1}^{Q} \theta_{1q} \Bigg\{ &\sum_{m=M+1}^{\infty} \frac{D_0 b_{mq}}{C_0 \bar{\alpha}_{m0}} e^{\bar{\alpha}_{m0}(b+x)} \cos\frac{m\pi y}{l} \operatorname{ch} k_0 (h+z) \\ &+ \sum_{m=1}^{\infty}\sum_{n=1}^{\infty} \frac{D_n b_{mq}}{C_n \bar{\alpha}_{mn}} e^{\bar{\alpha}_{mn}(b+x)} \cos\frac{m\pi y}{l} \cos\bar{k}_n (h+z) \Bigg\},\end{aligned} \tag{16}$$

where the coefficients $C_n$, $D_n$ and $b_{mq}$ are given by:

$$\begin{aligned} C_n &= \int_{-h}^{0} \operatorname{ch}^2 k_n (h+z)\, dz = \frac{1}{2}\left(h + \frac{g}{\omega^2}\operatorname{sh}^2 k_n h\right), \\ D_n &= \int_{-h}^{0} (z+h) \operatorname{ch} k_n (h+z)\, dz = \frac{1}{k_n^2} \\ &\left[\left(\frac{h\omega^2}{g} - 1\right)\operatorname{ch} k_n h + 1\right], \\ b_{mq} &= \frac{2}{l}\int_{(q-1)a}^{qa} \cos\frac{m\pi y}{l} dy = \frac{2}{m\pi} \\ &\left[\sin\frac{qm\pi}{Q} - \sin\frac{(q-1)m\pi}{Q}\right], \\ &q = 1, \ldots, Q, \;\; n = 0, \ldots, \infty, \;\; m = 1, \ldots, \infty. \end{aligned} \tag{17}$$

Expression (16) represents a sum of short crested evanescent waves.

### 3.2. $\phi^p, x \in [(p-1)L + b, pL - b], y \in [0, l], z \in [-h, 0], p = 1,..., P-1$

The wave potential $\phi^p$ in the domain between arrays $p$ and $p+1$ is governed by the following equation and boundary conditions:

$$\nabla^2 \phi^p = 0, \qquad x \in [(p-1)L + b, pL - b], \tag{18a}$$

$$\frac{\partial \phi^p}{\partial y} = 0, \qquad y = 0, \ y = l, \tag{18b}$$

$$\frac{\partial \phi^p}{\partial z} = 0, \qquad z = -h, \tag{18c}$$

$$\frac{\partial \phi^p}{\partial z} - \frac{\omega^2}{g}\phi^p = 0, \qquad z = 0, \tag{18d}$$

$$\frac{\partial \phi^p}{\partial x} = -i\omega (z+h)\theta_p(y), \qquad x = (p-1)L + b, \tag{18e}$$

$$\frac{\partial \phi^p}{\partial x} = -i\omega (z+h)\theta_{p+1}(y), \qquad x = pL - b. \tag{18f}$$

Also in this case we require the average in-phase motion of the gates to be null $\int_0^l \theta_p(y)\,dy = \int_0^l \theta_{p+1}(y)\,dy = 0$, i.e., we exclude long crested waves. For shorthand notation, define $x_p$ as follows:

$$x_p = x - b - (p-1)L \quad \text{for } p = 1, ..., P. \tag{19}$$

Imposing the boundary condition (18e) on the right side of array $p$ and (18f) on the left side of array $p+1$ and invoking orthogonality yields the expression for $\phi^p$:

$$\begin{aligned}
\phi^p = i\omega \sum_{q=1}^{Q} \Bigg\{ & \theta_{pq} \Bigg[ \sum_{m=1}^{M} \frac{D_0 b_{mq}}{\alpha_{m0} C_0} \frac{\cos \alpha_{m0}(x_p + 2b - L)}{\sin \alpha_{m0}(2b - L)} \cos \frac{m\pi y}{l} \operatorname{ch} k_0 (h+z) \\
& + \sum_{m=M+1}^{\infty} \frac{D_0 b_{mq}}{\overline{\alpha}_{m0} C_0} \frac{\operatorname{ch} \overline{\alpha}_{m0}(x_p + 2b - L)}{\operatorname{sh} \overline{\alpha}_{m0}(L - 2b)} \cos \frac{m\pi y}{l} \operatorname{ch} k_0 (h+z) \\
& + \sum_{m=1}^{\infty} \sum_{n=1}^{\infty} \frac{D_n b_{mq}}{\overline{\alpha}_{mn} C_n} \frac{\operatorname{ch} \overline{\alpha}_{mn}(x_p + 2b - L)}{\operatorname{sh} \overline{\alpha}_{mn}(L - 2b)} \cos \frac{m\pi y}{l} \cos \overline{k}_n (h+z) \Bigg] \\
& - \theta_{p+1,q} \Bigg[ \sum_{m=1}^{M} \frac{D_0 b_{mq}}{\alpha_{m0} C_0} \frac{\cos \alpha_{m0} x_p}{\sin \alpha_{m0}(2b - L)} \cos \frac{m\pi y}{l} \operatorname{ch} k_0 (h+z) \\
& + \sum_{m=M+1}^{\infty} \frac{D_0 b_{mq}}{\overline{\alpha}_{m0} C_0} \frac{\operatorname{ch} \overline{\alpha}_{m0} x_p}{\operatorname{sh} \overline{\alpha}_{m0}(L - 2b)} \cos \frac{m\pi y}{l} \operatorname{ch} k_0 (h+z) \\
& + \sum_{m=1}^{\infty} \sum_{n=1}^{\infty} \frac{D_n b_{mq}}{\overline{\alpha}_{mn} C_n} \frac{\operatorname{ch} \overline{\alpha}_{mn} x_p}{\operatorname{sh} \overline{\alpha}_{mn}(L - 2b)} \cos \frac{m\pi y}{l} \cos \overline{k}_n (h+z) \Bigg] \Bigg\}, \\
& p = 1, ..., P-1,
\end{aligned} \tag{20}$$

which is a summation of short-crested standing waves.

### 3.3. $\phi^+, x \in [(P-1)L + b, +\infty), y \in [0, l], z \in [-h, 0]$

The governing equation and boundary conditions are:

$$\nabla^2 \phi^+ = 0, \qquad x \in [(P-1)L + b, +\infty), \tag{21a}$$

$$\frac{\partial \phi^+}{\partial y} = 0, \qquad y = 0, \ y = l, \tag{21b}$$

$$\frac{\partial \phi^+}{\partial z} = 0, \qquad z = -h, \tag{21c}$$

$$\frac{\partial \phi^+}{\partial z} - \frac{\omega^2}{g}\phi^+ = 0, \qquad z = 0, \tag{21d}$$

$$\frac{\partial \phi^+}{\partial x} = -i\omega (z+h)\theta_P(y), \qquad x = (P-1)L + b, \tag{21e}$$

$$\phi^+ \text{ bounded as } x \to +\infty. \tag{21f}$$

With similar consideration to the previous case of $\phi^-$ we find the solution of problem (21a)–(21f) to be:

$$\begin{aligned}
\phi^+ = i\omega \sum_{q=1}^{Q} \theta_{Pq} \Bigg\{ & \sum_{m=M+1}^{\infty} \frac{D_0 b_{mq}}{C_0 \overline{\alpha}_{m0}} e^{-\overline{\alpha}_{m0} x_P} \cos \frac{m\pi y}{l} \operatorname{ch} k_0 (h+z) \\
& + \sum_{m=1}^{\infty} \sum_{n=1}^{\infty} \frac{D_n b_{mq}}{C_n \overline{\alpha}_{mn}} e^{-\overline{\alpha}_{mn} x_P} \cos \frac{m\pi y}{l} \cos \overline{k}_n (h+z) \Bigg\}.
\end{aligned} \tag{22}$$

### 3.4. Gate dynamics

Recalling definition (19) for $x_p$, conservation of angular momentum for each gate $j = 1,..., Q$ of each array $p = 1,..., P$ requires that:

$$\begin{aligned}
& I\ddot{\Theta}_{1j} + C\Theta_{1j} \\
& = -\int_{(j-1)a}^{ja} dy \int_{-h}^{0} \rho \left[ \Phi_t^- |_{x=-b} - \Phi_t^- |_{x1=0} \right] (z+h)\,dz, \\
& I\ddot{\Theta}_{pj} + C\Theta_{pj} \\
& = -\int_{(j-1)a}^{ja} dy \int_{-h}^{0} \rho \left[ \Phi_t^{p-1} |_{x_{p-1}=L-2b} - \Phi_t^p \Big|_{x_p=0} \right] (z+h)\,dz, \\
& p = 2, \ldots, P-1, \\
& I\ddot{\Theta}_{Pj} + C\Theta_{Pj} \\
& = -\int_{(j-1)a}^{ja} dy \int_{-h}^{0} \rho \left[ \Phi_t^{P-1} |_{x_{P-1}=L-2b} - \Phi_t^+ \Big|_{x_P=0} \right] (z+h)\,dz,
\end{aligned} \tag{23}$$

or equivalently, after the decomposition (9):

$$\begin{aligned}
& -\omega^2 I\theta_{1j} + C\theta_{1j} \\
& = \int_{(j-1)a}^{ja} dy \int_{-h}^{0} i\omega\rho \left[ \phi^- |_{x=-b} - \phi^1 |_{x_1=0} \right] (z+h)\,dz, \\
& -\omega^2 I\theta_{pj} + C\theta_{pj} \\
& = \int_{(j-1)a}^{ja} dy \int_{-h}^{0} i\omega\rho \left[ \phi^{p-1} |_{x_{p-1}=L-2b} - \phi^p |_{x_p=0} \right] (z+h)\,dz, \\
& p = 2, \ldots, P-1, \\
& -\omega^2 I\theta_{Pj} + C\theta_{Pj} \\
& = \int_{(j-1)a}^{ja} dy \int_{-h}^{0} i\omega\rho \left[ \phi^{P-1} |_{x_{P-1}=L-2b} - \phi^+ |_{x_P=0} \right] (z+h)\,dz.
\end{aligned} \tag{24}$$

$I$ is the moment of inertia of one gate about the hinge, $C$ is the net restoring torque. For small $\Theta$, $C$ can be expressed as:

$$C = \rho g (I_{xx}^A + I_z^V) - M_g g (z_g + h), \tag{25}$$

with:

$$I_{xx}^A = \int\int_{S_A} x^2\,dxdy, \quad I_z^V = \int\int\int_V (z+h)\,dV. \tag{26}$$

$S_A$ denotes cross sectional area of the gate at the water line and $V$ the water volume displaced by the gate in its rest vertical position. $M_g$ and $z_g$ are respectively the mass and the vertical coordinate of the center of mass of the gate. Substituting the expressions of the potential (16), (20) and (22) into Eq. (24), we obtain the momentum equation for each single gate $j = 1,..., Q$ of each array $p = 1,..., P$:

$$\left(-\omega^2 I + C\right)\theta_{1j} = \omega^2 \sum_{q=1}^{Q} \left\{ \theta_{1q} I_{1q}^{1j} + \theta_{2q} I_{2q}^{1j} \right\}, \tag{27a}$$

$$\left(-\omega^2 I + C\right)\theta_{pj} = \omega^2 \sum_{q=1}^{Q} \left\{ \theta_{p-1,q} I_{p-1,q}^{pj} + \theta_{pq} I_{pq}^{pj} + \theta_{p+1,q} I_{p+1,q}^{pj} \right\}, \tag{27b}$$
$$p = 2, \ldots, P-1,$$

$$\left(-\omega^2 I + C\right)\theta_{Pj} = \omega^2 \sum_{q=1}^{Q} \left\{ \theta_{P-1,q} I_{P-1,q}^{Pj} + \theta_{Pq} I_{Pq}^{Pj} \right\}. \tag{27c}$$

In Eqs. (27a) and (27c), $I_{1q}^{1j}$ ($I_{Pq}^{Pj}$) represents the added inertia of gate $G_{1j}$ ($G_{Pj}$) due to the unit rotation of the gate $G_{1q}$ ($G_{Pq}$):

$$I_{1q}^{1j} = I_{Pq}^{Pj} = \frac{\rho l}{2}\left[\sum_{m=1}^{M}\frac{D_0^2 b_{mq} b_{mj}}{C_0\alpha_{m0}\tan\alpha_{m0}(2b-L)} + \sum_{m=M+1}^{\infty}\frac{D_0^2 b_{mq} b_{mj}}{C_0\bar{\alpha}_{m0}}\left(1+\frac{1}{\mathrm{th}\,\bar{\alpha}_{m0}(L-2b)}\right) \sum_{m=1}^{\infty}\sum_{n=1}^{\infty}\frac{D_n^2 b_{mq} b_{mj}}{C_n\bar{\alpha}_{mn}}\left(1+\frac{1}{\mathrm{th}\,\bar{\alpha}_{mn}(L-2b)}\right)\right], \quad j,q=1,\ldots,Q, \tag{28}$$

with:

$$b_{mj} = \frac{2}{m\pi}\left[\sin\frac{jm\pi}{Q} - \sin\frac{(j-1)m\pi}{Q}\right]. \tag{29}$$

The fact that $I_{1q}^{1j} = I_{Pq}^{Pj}$ is due to the position of the 1 and $P$ arrays, which have one semi-infinite part of the channel on one side (respectively $-$ and $+$) and another array on the other side (respectively $p=2$ and $p=P-1$).

$I_{pq}^{pj}$ represents the added inertia of gate $G_{pj}$ due to the unit rotation of the gate $G_{pq}$:

$$I_{pq}^{pj} = \rho l\left[\sum_{m=1}^{M}\frac{D_0^2 b_{mq} b_{mj}}{C_0\alpha_{m0}\tan\alpha_{m0}(2b-L)} + \sum_{m=M+1}^{\infty}\frac{D_0^2 b_{mq} b_{mj}}{C_0\bar{\alpha}_{m0}\mathrm{th}\,\bar{\alpha}_{m0}(L-2b)} + \sum_{m=1}^{\infty}\sum_{n=1}^{\infty}\frac{D_n^2 b_{mq} b_{mj}}{C_n\bar{\alpha}_{mn}\mathrm{th}\,\bar{\alpha}_{mn}(L-2b)}\right], \quad j,q=1,\ldots,Q;\ \ p=2,\ldots,P-1. \tag{30}$$

$I_{p-1,q}^{pj}$ represents the added inertia of gate $G_{pj}$ due to the unit rotation of the gate $G_{p-1,q}$:

$$I_{p-1,q}^{pj} = -\frac{\rho l}{2}\left[\sum_{m=1}^{M}\frac{D_0^2 b_{mq} b_{mj}}{C_0\alpha_{m0}\sin\alpha_{m0}(2b-L)} + \sum_{m=M+1}^{\infty}\frac{D_0^2 b_{mq} b_{mj}}{C_0\bar{\alpha}_{m0}\mathrm{sh}\,\bar{\alpha}_{m0}(L-2b)} + \sum_{m=1}^{\infty}\sum_{n=1}^{\infty}\frac{D_n^2 b_{mq} b_{mj}}{C_n\bar{\alpha}_{mn}\mathrm{sh}\,\bar{\alpha}_{mn}(L-2b)}\right], \quad j,q=1,\ldots,Q;\ \ p=2,\ldots,P. \tag{31}$$

$I_{p+1,q}^{pj}$ represents the added inertia of gate $G_{pj}$ due to the unit rotation of the gate $G_{p+1,q}$. Because of the symmetry of the system, its expression is identical to (31), but for the index $p=1,\ldots,P-1$.

Eqs. (27a)–(27c) can be written in matrix form:

$$\left(-\omega^2 I + C\right)\mathbf{I}\{\theta\} = \mathbf{I}^a(\omega)\{\theta\}, \tag{32}$$

where $\{\theta\}$ is a column vector of length $s = P \times Q$ that contains all the angular displacements of the gates, as in (1) and (9):

$$\{\theta\} = \begin{Bmatrix}\{\theta_1\}\\ \vdots \\ \{\theta_p\}\\ \vdots \\ \{\theta_P\}\end{Bmatrix}. \tag{33}$$

$\mathbf{I}$ is the identity matrix of size $s \times s$. $\mathbf{I}^a(\omega)$ is a real banded symmetrical matrix of the added inertia also of size $s \times s$:

$$\mathbf{I}^a(\omega) = \begin{bmatrix} \mathbf{I}_1^1 & \mathbf{I}_2^1 & & & \\ \mathbf{I}_1^2 & \mathbf{I}_2^2 & \mathbf{I}_3^2 & & 0 \\ & \ddots & \ddots & \ddots & \\ & & \mathbf{I}_{P-2}^{P-1} & \mathbf{I}_{P-1}^{P-1} & \mathbf{I}_P^{P-1} \\ & 0 & & \mathbf{I}_{P-1}^{P} & \mathbf{I}_P^{P} \end{bmatrix}, \tag{34}$$

where each $\mathbf{I}_p^p$, is a symmetrical square matrix of size $Q \times Q$:

$$\mathbf{I}_p^p = \begin{bmatrix} I_{p1}^{p1} & \cdots & I_{pQ}^{p1} \\ \vdots & \ddots & \vdots \\ I_{p1}^{pQ} & \cdots & I_{pQ}^{pQ} \end{bmatrix}. \tag{35}$$

The bandwidth of $\mathbf{I}^a(\omega)$ is $3Q$, which is consistent with the fact that each angular displacement of the $p-th$ array is hydrodynamically coupled with its neighboring arrays, $p-1$ and $p+1$.

### 3.5. Eigenfrequencies and eigenvectors

The system (32) is equivalent to a $s = P \times Q$ degree-of-freedom system with given masses and stiffness. Hence the eigenfrequencies $\omega$ can be determined by solving the following implicit non linear eigen-value condition:

$$\left|\left(-\omega^2 I + C\right)\mathbf{I} + \mathbf{I}^a(\omega)\right| = 0. \tag{36}$$

Once the eigenfrequencies are found, the corresponding modal forms can be obtained setting the displacement of the gate $G_{11} = 1$ and then solving the linear system (32).

## 4. In-phase motion

We now let:

$$\Theta_p(t) = \Theta_{p1}(t) = \ldots = \Theta_{pQ}(t) \quad \text{for } p = 1,\ldots,P. \tag{37}$$

Note that each $\Theta_p$ is now constant in $y$, like if each gate within the $p$th array have been locked to each other. This type of motion allows to study the problem in the two dimensional vertical plane $(x, z)$.

### 4.1. $\phi^-, x \in (-\infty, -b], z \in [-h, 0]$

Without the $y$ dependence, the governing equation and boundary conditions are:

$$\nabla^2\phi^- = 0, \qquad x \in (-\infty, -b], \tag{38a}$$

$$\frac{\partial\phi^-}{\partial z} = 0, \qquad z = -h, \tag{38b}$$

$$\frac{\partial\phi^-}{\partial z} - \frac{\omega^2}{g}\phi^- = 0, \qquad z = -0, \tag{38c}$$

$$\frac{\partial\phi^-}{\partial x} = -i\omega(z+h)\theta_1, \qquad x = -b. \tag{38d}$$

Because waves propagate to $-\infty$, the solution for $\phi^-$ is made only of propagating and evanescent long crested waves:

$$\phi^- = \sum_{n=0}^{\infty}\theta_1\frac{\omega D_n}{k_n C_n}e^{-ik_n(b+x)}\mathrm{ch}\,k_n(h+z). \tag{39}$$

*4.2. $\phi^p, x \in [(p-1)L + b, pL - b], z \in [-h, 0], p = 1,..., P-1$*

The wave potential $\phi^p$ is governed by the following equation and boundary conditions:

$$\nabla^2\phi^p = 0, \qquad x \in [(p-1)L + b, pL - b], \tag{40a}$$

$$\frac{\partial\phi^p}{\partial z} = 0, \qquad z = -h, \tag{40b}$$

$$\frac{\partial\phi^p}{\partial z} - \frac{\omega^2}{g}\phi^p = 0, \qquad z = 0, \tag{40c}$$

$$\frac{\partial\phi^p}{\partial x} = -i\omega(z+h)\theta_p, \qquad x = (p-1)L + b, \tag{40d}$$

$$\frac{\partial\phi^p}{\partial x} = -i\omega(z+h)\theta_{p+1}, \qquad x = pL - b. \tag{40e}$$

Solution of (40a)–(40e) is:

$$\phi^p = \sum_{n=0}^{\infty} \frac{i\omega D_n}{k_n C_n} \left\{ \theta_p \frac{\cos k_n(x_p + 2b - L)}{\sin k_n(2b-L)} - \theta_{p+1} \frac{\cos k_n x_p}{\sin k_n(2b-L)} \right\} \operatorname{ch} k_n(h+z), \tag{41}$$

which is a summation of standing long crested waves in $x$.

*4.3. $\phi^+, x \in [(P-1)L + b, +\infty), z \in [-h, 0]$*

The governing equation and boundary conditions are:

$$\nabla^2\phi^+ = 0, \qquad x \in [(P-1)L + b, \tag{42a}$$

$$\frac{\partial\phi^+}{\partial z} = 0, \qquad z = -h, \tag{42b}$$

$$\frac{\partial\phi^+}{\partial z} - \frac{\omega^2}{g}\phi^+ = 0, \qquad z = 0, \tag{42c}$$

$$\frac{\partial\phi^+}{\partial x} = -i\omega(z+h)\theta_P, \qquad x = (P-1)L + b. \tag{42d}$$

This case includes only positive $x$-propagating and evanescent long crested waves:

$$\phi^+ = -\sum_{n=0}^{\infty} \theta_P \frac{\omega D_n}{k_n C_n} e^{ik_n x_P} \operatorname{ch} k_n(h+z). \tag{43}$$

*4.4. Gate dynamics*

Because of the in-phase motion, it suffices to consider the dynamics of one gate of the $p$th array rather than the entire array. For harmonic motion, conservation of angular momentum requires:

$$\begin{aligned}
&-\omega^2 I\theta_1 + C\theta_1 \\
&= \int_0^a dy \int_{-h}^0 i\omega\rho \left[ \phi^-|_{x=-b} - \phi^1|_{x_1=0} \right](z+h)\,dz, \\
&-\omega^2 I\theta_p + C\theta_p \\
&= \int_0^a dy \int_{-h}^0 i\omega\rho \left[ \phi^{p-1}|_{x_{p-1}=L-2b} - \phi^p|_{x_P=0} \right](z+h)\,dz, \\
&p = 2, \ldots, P-1, \\
&-\omega^2 I\theta_P + C\theta_P \\
&= \int_0^a dy \int_{-h}^0 i\omega\rho \left[ \phi^{P-1}|_{x_{P-1}=L-2b} - \phi^+|_{x_P=0} \right](z+h)\,dz.
\end{aligned} \tag{44}$$

Substituting the expressions of the potentials (39), (41) and (43) into the equations above, we obtain:

$$\begin{aligned}
&\left(-\omega^2 I + C\right)\theta_1 = i\omega D\theta_1 + \omega^2 \left\{ \theta_1 I_1^1 + \theta_2 I_2^1 \right\}, \\
&\left(-\omega^2 I + C\right)\theta_p = \omega^2 \left\{ \theta_{p-1} I_{p-1}^p + \theta_p I_p^p + \theta_{p+1} I_{p+1}^p \right\}, \; p = 2, \ldots, P-1, \\
&\left(-\omega^2 I + C\right)\theta_P = i\omega D\theta_P + \omega^2 \left\{ \theta_{P-1} I_{P-1}^P + \theta_P I_P^P \right\},
\end{aligned} \tag{45}$$

where the term $D$ is the radiation damping coefficient $D = \omega\rho a(D_0^2/k_0 C_0)$, while the added inertia are defined by:

$$\begin{aligned}
&I_1^1 = I_P^P = \rho a \left\{ \frac{D_0^2}{k_0 C_0 \tan k_0(2b-L)} + \sum_{n=1}^{\infty} \frac{D_n^2}{k_n C_n} \left[ 1 + \frac{1}{\operatorname{th} k_n(L-2b)} \right] \right\}, \\
&I_p^p = 2\rho a \sum_{n=0}^{\infty} \frac{D_n^2}{k_n C_n \tan k_n(2b-L)}, \; p = 2, \ldots, P-1, \\
&I_{p-1}^p = -\rho a \sum_{n=0}^{\infty} \frac{D_n^2}{k_n C_n \sin k_n(2b-L)}, \; p = 2, \ldots, P, \\
&I_{p+1}^p = I_{p-1}^p, \; p = 1, \ldots, P-1.
\end{aligned} \tag{46}$$

In matrix form, system (45) can be written as:

$$\left(-\omega^2 I + C\right)\mathbf{I}\{\theta\} = \tilde{\mathbf{I}}^a(\omega)\{\theta\}, \tag{47}$$

where $\{\theta\}$ is now a column vector of length $P$:

$$\{\theta\} = \begin{Bmatrix} \theta_1 \\ \vdots \\ \theta_P \end{Bmatrix}. \tag{48}$$

$\mathbf{I}$ is the identity matrix of size $P \times P$, and $\tilde{\mathbf{I}}^a(\omega)$ is a banded symmetrical matrix also of size $P \times P$:

$$\tilde{\mathbf{I}}^a(\omega) = \begin{bmatrix} I_1^1 - i\omega D & I_2^1 & & & 0 \\ I_1^2 & I_2^2 & I_3^2 & & \\ & \ddots & \ddots & \ddots & \\ & & I_{P-2}^{P-1} & I_{P-1}^{P-1} & I_P^{P-1} \\ 0 & & & I_{P-1}^P & I_P^P - i\omega D \end{bmatrix}. \tag{49}$$

$\tilde{\mathbf{I}}^a(\omega)$ is not yet a real added inertia matrix, as it still contains a damping term in the first and last row (see expression (49)).

*4.5. Eigenfrequencies and eigenvectors*

Eq. (45) are equivalent to a damped $P$ degree-of-freedom system with given masses and stiffness. We can find the eigenfrequencies by omitting damping, i.e. posing $D = 0$. Hence the added inertia matrix (49) becomes real:

$$\mathbf{I}^a(\omega) = \begin{bmatrix} I_1^1 & I_2^1 & & & \\ I_1^2 & I_2^2 & I_3^2 & & 0 \\ \ddots & \ddots & \ddots & & \\ & I_{P-2}^{P-1} & I_{P-1}^{P-1} & I_P^{P-1} & \\ 0 & & I_{P-1}^P & I_P^P & \end{bmatrix}. \tag{50}$$

The eigenfrequencies $\omega$ can be determined from the eigen-value condition:

$$\left|\left(-\omega^2 I + C\right)\mathbf{I} - \mathbf{I}^a(\omega)\right| = 0. \tag{51}$$

The corresponding eigenvectors can be found by setting the displacement of the gate $G_{11} = 1$.

## 5. Numerical results

With reference to Fig. 1, we consider a $P = 3$, $Q = 5$ gate farm. The following gate and channel characteristics are chosen for numerical investigation:

*5.1. Out-of-phase motion*

Numerical solution of eigenvalue condition (36) gives $P \times (Q-1) = 12$ roots. The numerical values of the eigenfrequencies are listed in Table 1. The respective modal forms are shown in Figs. 2 and 3 where the number near each gate represents the angular displacement relative to $\theta_{11} = 1$. Let $K$ indicates the number of gates of the

| Parameter | Symbol | Value |
|---|---|---|
| Gate width | $a$ | 6 m |
| Gate thickness | $2b$ | 1.5 m |
| Distance between arrays | $L$ | 10 m |
| Moment of inertia | $I$ | 72000 kg m$^2$ |
| Buoyancy restoring torque | $C$ | 950000 kg m$^2$ s$^{-2}$ |
| Gate mass | $M_g$ | 5200 kg |
| Water depth | $h$ | 5 m |
| Density of water | $\rho$ | 1000 kg m$^{-3}$ |

**Table 1**
Natural frequencies of trapped modes.

| $\omega$ (1/s) | Period (s) | $K$ | Mode |
|---|---|---|---|
| 1.0012 | 6.2725 | 2.5 | $N_{11}$ |
| 0.9859 | 6.3698 | 2.5 | $N_{12}$ |
| 0.9712 | 6.4662 | 2.5 | $N_{13}$ |
| 0.8838 | 7.1057 | $3.\overline{3}$ | $N_{21}$ |
| 0.8451 | 7.4311 | $3.\overline{3}$ | $N_{22}$ |
| 0.8108 | 7.7454 | $3.\overline{3}$ | $N_{23}$ |
| 0.7448 | 8.4318 | 5 | $N_{31}$ |
| 0.6589 | 9.5310 | 5 | $N_{32}$ |
| 0.5954 | 10.5475 | 5 | $N_{33}$ |
| 0.5540 | 11.3357 | 10 | $N_{41}$ |
| 0.4058 | 15.4756 | 10 | $N_{42}$ |
| 0.3273 | 19.1873 | 10 | $N_{43}$ |

**Table 2**
Limiting values of eigenfrequencies as $L \to \infty$, equal to Li and Mei [14].

| $\omega$ (1/s) | Period (s) | $K$ | Mode |
|---|---|---|---|
| 0.9869 | 6.3666 | 2.5 | $N_1$ |
| 0.8476 | 7.4129 | $3.\overline{3}$ | $N_2$ |
| 0.6699 | 9.3793 | 5 | $N_3$ |
| 0.4470 | 14.0563 | 10 | $N_4$ |

first array ($p = 1$) per modal wave length. Table 1 shows that, as $K$ increases, the natural frequency decreases. Figs. 2a–d and 3a–d show that for modes $N_{11}$, $N_{21}$, $N_{31}$, and $N_{41}$, each array has the same modal shape, but for the central array ($p = 2$) where gates have larger oscillation amplitudes. Figs. 2b–e and 3b–e show modes $N_{12}$, $N_{22}$, $N_{32}$, and $N_{42}$: they are characterized by having the middle array ($p = 2$) with null angular displacement, while the last array ($p = 3$) is in opposite phase with respect to the first ($p = 1$). Figs. 2c–f and 3c–f represent the remaining modes $N_{13}$, $N_{23}$, $N_{33}$, and $N_{43}$: modal deformation is the same, but for the middle array ($p = 2$) which is in opposition of phase with the other two. Consider now the parametric dependence on $L$. Fig. 4 shows the dependence of the eigenfrequencies from the distance $L$ between arrays. We find that the eigenfrequencies tend to the same values of Li and Mei [14] as $L \to \infty$. Indeed, the 12 natural modes of Table 1, degenerate to $(Q-1) = 4$ modes $N_1$, $N_2$, $N_3$ and $N_4$. The values of the eigenfrequencies are listed in Table 2, while Fig. 5 indicates the angular displacements of the gates.

### 5.2. In-phase motion

Let $\det(\omega)$ be the left-hand side of the eigen-value condition (51). Recalling that $I_1^1 = I_3^3$, and, $I_2^1 = I_1^2 = I_3^2 = I_2^3$, the expression of $\det(\omega)$ for $P = 3$ has an explicit form:

$$det(\omega) = \left[-\omega^1\left(I + I_1^1\right) + C\right] \times \left\{2\left(\omega^2 I_2^1\right)^2 - \left[-\omega^2\left(1 + I_1^1\right) + C\right]\left[-\omega^2\left(I + I_2^2\right) + C\right]\right\}. \quad (52)$$

Fig. 6 depicts the graph of $\det(\omega)$ vs. $\omega$. The plot shows that there are $\infty$ discrete zeros of $\det(\omega)$; hence, $\infty$ discrete eigenfrequencies are

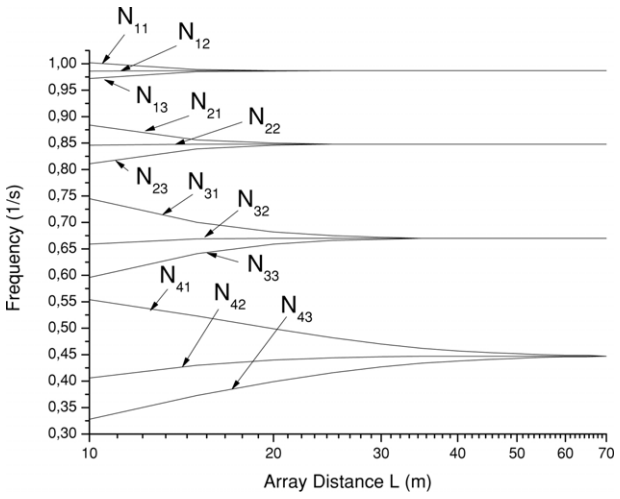


**Fig. 4.** Eigenfrequencies vs. the distance $L$ for the different modal shapes $N$. For large $N$ the eigenfrequencies become the same of Li and Mei [14].

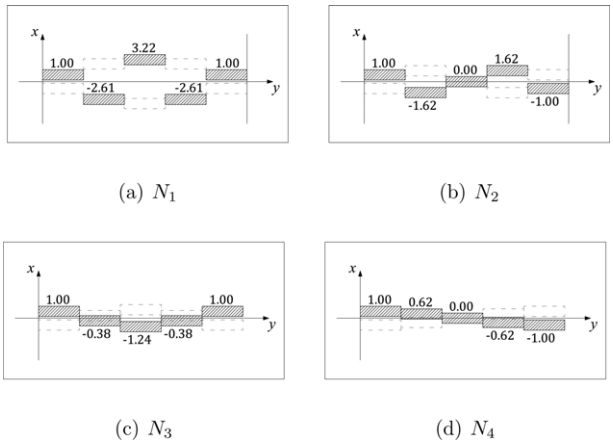


(a) $N_1$ (b) $N_2$

(c) $N_3$ (d) $N_4$

**Fig. 5.** Modal profiles for $L \to \infty$, equal to Li and Mei [14].

possible. Indeed, from expression (52) it is easily seen that equation $\det(\omega) = 0$ can be satisfied by three sub-conditions for $\omega$:

$$\omega^2 I_2^1 - \sqrt{\frac{\left[-\omega^2\left(I + I_1^1\right) + C\right]\left[-\omega^2\left(I + I_2^2\right) + C\right]}{2}} = 0, \quad (53a)$$

$$-\omega^2\left(I + I_1^1\right) + C = 0, \quad (53b)$$

$$\omega^2 I_2^1 - \sqrt{\frac{\left[-\omega^2\left(I + I_1^1\right) + C\right]\left[-\omega^2\left(I + I_2^2\right) + C\right]}{2}} = 0. \quad (53c)$$

Let $\omega_1 = (\omega_{11},..., \omega_{1\infty})$ represent all the infinite roots of (53a). Similarly, let $\omega_2 = (\omega_{21},..., \omega_{2\infty})$ represent all the infinite roots of (53b), and $\omega_3 = (\omega_{31},..., \omega_{3\infty})$ for (53c). Fig. 6 shows the first 11 roots of $\det(\omega) = 0$. For $j = 1, 2$, Table 3 shows the numerical values of $\omega_{1j}$, $\omega_{2j}$ and $\omega_{3j}$, while the modal forms $N(\omega_{1j})$, $N(\omega_{2j})$ and $N(\omega_{3j})$, associated to $\omega_{1j}$, $\omega_{2j}$ and $\omega_{3j}$ are shown in Fig. 7. From inspection of Fig. 7, we evince that: the modal forms $N(\omega_{11}) - N(\omega_{32})$ are characterized by three arrays in phase; the modal forms $N(\omega_{21}) - N(\omega_{22})$ are identical, and are characterized by the middle array ($p = 2$) with zero angular displacement while the arrays $p = 1$ and $p = 3$ in opposition of phase. Finally the modal forms $N(\omega_{31}) - N(\omega_{12})$ are characterized by the middle array ($p = 2$) in opposite phase with respect to the first ($p = 1$) and the last array ($p = 3$).

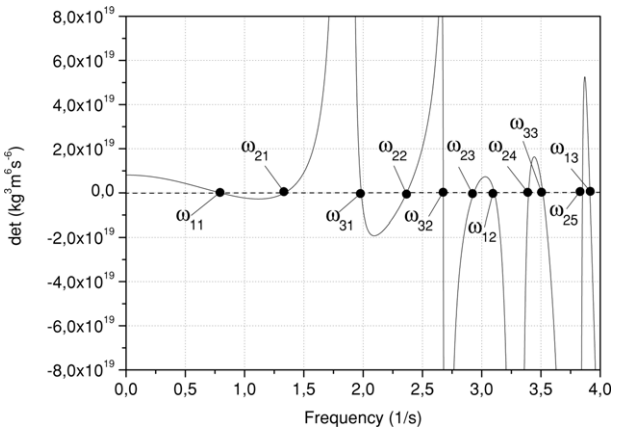


**Fig. 6.** Function det($\omega$) and first 11 eigenfrequencies.

**Table 3**
Natural frequencies $\omega_{1j}$, $\omega_{2j}$ and $\omega_{3j}$, for $j = 1, 2$.

| $j$ | $\omega_{1j}$ (1/s) | $\omega_{2j}$ (1/s) | $\omega_{3j}$ (1/s) |
|---|---|---|---|
| 1 | 0.795 | 1.339 | 1.985 |
| 2 | 3.108 | 2.368 | 2.676 |

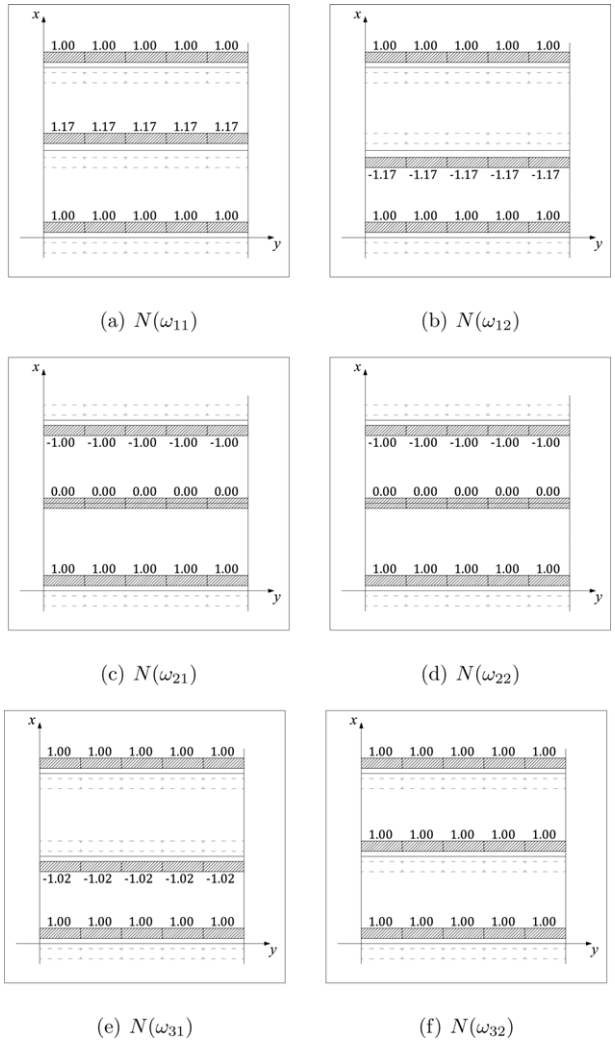


(a) $N(\omega_{11})$ (b) $N(\omega_{12})$

(c) $N(\omega_{21})$ (d) $N(\omega_{22})$

(e) $N(\omega_{31})$ (f) $N(\omega_{32})$

**Fig. 7.** Modal profiles of the in-phase motion.

## 6. Conclusions

A solution of the natural modes for a $P \times Q$ gate farm WEC in a infinitely long channel has been obtained. We have considered both cases of out-of-phase motion and in-phase motion. In the first case, $P \times (Q-1)$ eigenfrequencies have been found, while considering in-phase motion, we obtain an infinite set of $\omega$ that satisfy the eigenvalue condition. For the out-of-phase motion, when the distance between arrays is very large, the eigenfrequencies of the gate farm converge to the eigenfrequencies of the single array analyzed by Li and Mei [14]. Comparing the modal forms of the gate farm with those of a single array, we have shown that the overall angular displacement is larger due to the effect of the added inertia trapped between the arrays. In the present theory we kept into account the effect of thickness by relaxing the "thin-gate" hypothesis of Renzi and Dias [6–9]. The theory developed here suggests that the optimal WEC should be designed such that there are no propagating short crested wave ($M = 0$) for each modal oscillation. A linear theory for a gate farm in open sea that includes damping term due to wave radiation, is being developed. This will allow quantification of the resonating response and evaluation of the increased potential in terms of power extraction from incident waves.

## Acknowledgements

The authors wish to thank Giorgio Bellotti and Ali Abdolali of Università degli Studi Roma Tre for fruitful discussions.

## References

[1] McCormick ME. Ocean wave energy conversion. Dover; 2007.
[2] Cruz J. Ocean wave energy. Springer; 2008.
[3] Whittaker T, Collier D, Folley M, Osterried M, Henry A, Crowley M. . The development of Oyster: a shallow water surging wave energy converter. In: 7th European Wave and Tidal Energy Conference, Porto, Portugal. 2007.
[4] Consorzio Venezia Nuova. Study on the influence of the inclination angle and the gate shape on gate response. Technical report Studio 2.2.10 by Delft Hydraulics; November 1988.
[5] Renzi E, Abdolali A, Bellotti G, Dias F. . Mathematical modelling of the oscillating wave surge converter. In: Proceedings of the 33rd conference of hydraulics and hydraulic engineering, Brescia, Italy. 2012.
[6] Renzi E, Dias F. Resonant behaviour of an oscillating wave energy converter in a channel. Journal of Fluid Mechanics 2012;701:482–510.
[7] Renzi E, Dias F. Hydrodynamics of the oscillating wave surge converter in the open ocean. European Journal of Mechanics B/Fluids 2013;41:1–10.
[8] Renzi E, Dias F. Relations for a periodic array of flap-type wave energy converters. Applied Ocean Research 2012;39:31–9.
[9] Renzi E, Dias F. Resonant scattering by a periodic array of plates with application to wave energy extraction. Proceedings of the IWWWFB27 2012:157–60.
[10] Mei CC, Sammarco P, Chan ES, Procaccini C. Subharmonic resonance of proposed storm gates for Venice lagoon. Proceedings of the Royal Society of London A 1994;444:257–65.
[11] Sammarco P, Tran H, Mei CC. Subharmonic resonance of Venice storm gates in waves. I. Evolution equation and uniform incident waves. Journal of Fluid Mechanics 1997;349:295–325.
[12] Sammarco P, Tran H, Gottlieb O, Mei CC. Subharmonic resonance of Venice storm gates in waves. II. Sinusoidally modulated incident waves. Journal of Fluid Mechanics 1997;349:327–59.
[13] Adamo A, Mei CC. Linear response of Venice storm gates to incident waves. Proceedings of the Royal Society of London A 2005;461:1711–34.
[14] Li G, Mei CC. Natural modes of mobile flood gates. Applied Ocean Research 2003;25:115–26.
[15] Panizzo A, Sammarco P, Bellotti G, De Girolamo P. EOF analysis of complex response of Venice mobile gates. Journal of Waterway, Port, Coastal, and Ocean Engineering 2006;132:172–9.